

A Probabilistic Quantification of Galaxy Cluster Membership

R.J. Brunner and L.M. Lubin¹

*Department of Astronomy, California Institute of Technology,
MC 105-24, Pasadena, CA 91125*

`rb@astro.caltech.edu`

ABSTRACT

Clusters of galaxies are important laboratories for understanding both galaxy evolution and constraining cosmological quantities. Any analysis of clusters, however, is best done when one can reliably determine which galaxies are members of the cluster. While this would ideally be done spectroscopically, the difficulty in acquiring a complete sample of spectroscopic redshifts becomes rather daunting, especially at high redshift where the background contamination becomes increasingly larger. Traditionally, an alternative approach of applying a statistical background correction has been utilized, which, while useful in a global sense, does not provide information for specific galaxies. In this paper, we develop a more robust technique which uses photometrically estimated redshifts to determine cluster membership. This technique can either be used as an improvement over the commonly used statistical correction method or it can be used to determine cluster candidates on an individual galaxy basis. By tuning the parameters of our algorithm, we can selectively maximize our completeness or, alternatively, minimize our contamination. Furthermore, our technique provides a statistical quantification of both our resulting completeness and contamination from foreground and background galaxies.

Subject headings: galaxies: distances and redshifts and clusters: general; cosmology: observations

1. Introduction

In the wake of the Hubble deep field campaigns (Williams *et al.* 1996), and with the growth of large photometric surveys (*e.g.*, DPOSS, SDSS, *etc.*), the techniques involved in calculating

¹Hubble Fellow

photometric redshifts have become increasingly more sophisticated and precise (see Weymann *et al.* 1999, for a recent synopsis of the field). Accuracies of $\sigma_z = 0.05$ can be routinely achieved (Brunner *et al.* 1999). Therefore, it is now possible to use photometric redshifts to answer specific scientific questions (*e.g.*, Connolly *et al.* 1998; Brunner *et al.* 2000). In light of this, we have begun a program to use accurate photometric redshifts to study the galaxy populations in high-redshift clusters of galaxies. For this study, we have examined the most well-studied sample of optically-selected, high-redshift clusters to date – that of Oke, Postman & Lubin (1998). Over the past few years, Oke *et al.* (1998) have undertaken a detailed photometric, spectroscopic, and morphological survey of nine candidate clusters at $z \gtrsim 0.6$. The survey consists of deep *BVR_IK'* photometry, over 130 low-resolution Keck spectra per cluster field, and high-spatial-resolution WFPC2 imagery from the *Hubble Space Telescope* (HST).

Previous work on similar galaxy cluster samples at various redshifts has relied on statistical corrections in order to remove contamination due to field galaxies when spectroscopic identifications are not available for all galaxies in the cluster field (*e.g.*, Aragón-Salamanca *et al.* 1993; Lubin 1996; Smail *et al.* 1997; Dressler *et al.* 1997; Couch *et al.* 1998; Stanford *et al.* 1998; Lubin *et al.* 1998). These types of corrections, however, are fraught with potential systematic effects, including cosmological variance, weak lensing, and sample selection criteria. While these effects will only serve to increase the noise of any measurement made over a statistically complete sample, they will systematically affect any measurements made on an individual cluster (*e.g.*, the Morphological fraction or the Morphology-Density relationship), introducing a bias into the actual measurement process. Furthermore, these line-of-sight contamination corrections apply to the entire galaxy sample and do not provide any information for specific galaxies. As a result, we have decided to explore the role photometric redshifts could play in improving the reliability of identifying galaxy cluster members (Kodama *et al.* 1999; Lubin & Brunner 1999).

In this paper, we first describe in Section 2 the details of the data observations, reduction, and catalog generation, emphasizing relevant points which are important for the estimation of photometric redshifts. In Section 3 we describe the details of our redshift estimation technique. Next, we detail the cluster galaxy identification procedure in Section 4. We conclude with a discussion of our results and future applications.

2. Data

For the photometric redshift analysis, we have used the photometric and spectroscopic data from the original cluster survey of Oke *et al.* (1998). This survey consists of nine candidate clusters at redshifts of $z \gtrsim 0.6$: Cl 0023+0423, Cl 0231+0048, Cl 0943+4804, Cl 1324+3011, Cl 1325+3009, Cl 1604+4304, Cl 1604+4321, Cl 1607+4109, and Cl 2157+0347. Oke *et al.* (1998) have determined that six of the nine candidate clusters are indeed real density enhancements, consistent with that of a cluster of galaxies. The observational data relevant for the work described in this paper consists of *B*, *V*, *R*, *I*, and *K'* band imaging and spectroscopic observations of selected galaxies in each

field.

2.1. Observations and Data Reduction

All of the ground-based optical observations, both broad band and spectroscopic, were taken with the Low Resolution Imaging Spectrometer (LRIS; Oke *et al.* 1995) on either the Keck I or the Keck II 10-m telescopes. The infrared imaging was performed with the Infrared Imaging Camera (IRIM) on the Mayall 4-m telescope at Kitt Peak National Observatory. In this section, we briefly describe the observations and the data reduction; however, the reader is referred to Oke *et al.* (1998) for a complete account of these observations.

2.1.1. Broad-Band Optical

The photometric survey was conducted in four broad band filters, *BVRI*, which closely match the Cousins system. The response curves of these filters are shown in Figure 1 of Oke *et al.* (1998). In imaging mode, LRIS covers a field-of-view of 6×8 arcmin. The total exposure times in each filter are 3600, 2000, 1200, and 900 seconds for *B*, *V*, *R*, and *I*, respectively, and were chosen to give fairly uniform errors in the photometry. The *B*, *V*, and *R* observations consisted of two equal exposures to allow for accurate cosmic ray rejection. The *I* exposure time was broken into 3 equal exposures in order to cope with the cosmic rays, as well as to avoid approaching the CCD saturation level.

The LRIS imaging data were reduced in the standard fashion. All frames were bias-subtracted, and pixel-to-pixel sensitivity variations were removed using dome flats. Large-scale gradients were removed by dividing each frame by a normalized two-dimensional spline fit to the sky values in a sky-flat. The sky-flat was created by generating a median image from a stack of frames for each night and passband. For the *I* band data, a two-dimensional fringe map was also created from the median filtered image by removing large-scale gradients within the median image. Fringing was removed from each *I* band frame by subtracting a suitably scaled version of the fringe map.

Image registration for a given cluster field was performed by identifying approximately 10 unsaturated stars (detectable in all 4 passbands) to be used as astrometric reference points. The mean *X* and *Y* offsets of these stars in every frame taken of the cluster were computed relative to their locations in a fiducial *B* band image. All image data for the cluster were shifted to match the *B* band coordinate system using a flux conserving Lagrangian interpolation scheme to achieve registration at the sub-pixel level. Once all frames of a given cluster were registered to a common coordinate system, the independent exposures in each passband were co-added to produce the final four *BVRI* images.

The Keck imaging has been calibrated to the standard Cousins-Bessell-Landolt (Cape) system

through exposures of a number of Landolt standard star fields (Landolt 1992). For a circular aperture with a radius of $3''$, the approximate limiting magnitudes are $B = 25.1$, $V = 24.1$, $R = 23.5$, and $I = 21.7$ for a $5\text{-}\sigma$ detection.

2.1.2. Spectroscopic

Multi-slit observations of the cluster field were made with LRIS in spectroscopic mode using a 300 g mm^{-1} grating blazed at 5000 \AA . The chosen grating provided a dispersion of 2.35 \AA per pixel and a spectral coverage of 5100 \AA . The grating angle was set in order to provide coverage from approximately 4400 \AA to 9500 \AA in the first order. A GG495 glass filter was used to eliminate the overlapping second order spectrum; there is, therefore, no second order contamination below 9700 \AA . In order to obtain the full wavelength range along the dispersion axis, the field-of-view of the spectral observations was reduced from that of the imaging mode to approximately $2 \times 8\text{ arcmin}$.

Spectroscopic candidates were chosen from preliminary R band imaging of each cluster field. All objects brighter than approximately $R = 23.5 \pm 0.1$ within the spectroscopic field-of-view of LRIS were included as candidates for slit-mask spectra. For each cluster field, six different slit-masks were made with approximately 30 objects per mask (including guide stars and duplicate observations). The exposure time for each mask was 1 hour. Flat-fielding and wavelength calibration were performed using internal flat-field and arc lamp exposures which were taken after each science exposure.

In practice, about 130 spectra were acquired per cluster field, with ~ 100 yielding measurable redshifts. A redshift measurement procedure which relies, in part, on visual inspection was used. The quality of the redshift identification was ranked with a number from 1 to 4, which roughly corresponds to the number of features used to identify the redshift. A quality of 4 means that the redshift is certain; a quality of 1 means that only one emission line was observed, and the redshift is only possible. Because the fore/background contamination rate is so large at our cluster redshifts, approximately 50 – 85% of the galaxies turn out to be field galaxies, rather than cluster members (Oke *et al.* 1998; Postman *et al.* 1998, 2000).

2.1.3. Infrared

Deep infrared imaging of the cluster sample was taken with IRIM which contains a 256×256 NICMOS3 HgCdTe array and has a resolution of 0.60 arcsecond per pixel on the 4-m telescope. The field-of-view ($154 \times 154\text{ arcseconds}$) covers the central region of each cluster. In order to make the deepest possible observations over this region the entire LRIS field-of-view was not mosaiced. Observations were made in the $2.2\mu K'$ band. Each central field was observed using a 4×4 dither pattern with a stepsize of $10''$ and a total extent of $30''$. Each exposure had an effective exposure time of 1 minute, with 4 co-additions of individual, background-limited 15 second integrations.

The total integration time on an individual cluster varied between 3 and 4.4 hours. Because the fields were not excessively crowded, we were able to use in-field dithering to create a global sky flat.

The K' cluster data were reduced using the Deep Infrared Mosaicing Software (DIMSUM), a publicly available package of IRAF scripts. This software generates not only a final stacked image but also a corresponding exposure image, where each pixel encodes the total number of seconds in the corresponding stacked image. This exposure image was appropriately scaled and used as a weight image by SExtractor during the catalog generation (see §2.2).

The data were linearized, trimmed to exclude masked columns and rows on the edges of the arrays, and dark-subtracted using dark frames of the same exposure length as the observations. All images of a given night were flattened by a super flat made from a series of dome flats taken during the previous day. As part of the DIMSUM procedure, sky subtraction was done by subtracting a scaled median of nine temporally adjacent exposures for each frame. A first-pass reduction was used to create an object mask for each frame. This mask was created from a fully stacked mosaic image. It therefore excluded not only the bright objects, but also those objects too faint to be detected in an individual exposure. In the second pass, the object mask was used to avoid object contamination of the sky flat in the production of sky frames. Final mosaicing of the images of each cluster were made with a replication of each pixel by a factor of 4 in both dimensions. This procedure conserves flux while eliminating the need for interpolation when the individual frames are co-aligned. A bad pixel mask was used to exclude bad pixels from the final summed images.

Absolute photometric transformations were derived from the observations of Persson *et al.* (1998) HST standard stars. Each standard star was observed every night in five separate array positions. The observations of the standard stars were reduced in a similar manner to the cluster data (see Oke *et al.* 1998). An approximate limiting magnitude of $K' = 20$ for a 5σ detection was reached in a standard aperture of radius $3''.0$.

2.2. Catalog Generation

We used SExtractor version 2.1.5 (Bertin & Arnouts 1996) to perform the source detection and photometry because this program is able to detect objects in one image and analyze the corresponding pixels in a separate image. Applied uniformly to multi-band image data (i.e. use the same detection image for all measurement images), this method will produce a matched aperture photometric catalog. We generated an optimal detection image from the B , V , R , & I images using a χ^2 process (Szalay *et al.* 1998). Briefly, this process involves convolving each input image with a Gaussian kernel matched to the seeing. The convolved images were squared and normalized so that they have zero mean and unit variance. The four processed images (corresponding to the original B , V , R , & I images) were coadded, forming the χ^2 detection image.

In order to determine the optimal threshold parameters for source detection, we compared a histogram of the pixel distribution in the χ^2 image with a χ^2 function with four degrees of freedom.

(This distribution theoretically corresponds to the background pixel distribution for our coadded χ^2 image.) By taking the difference between the two histograms (pixel minus theory), we generated the histogram of pixel values which were due to the objects that we were trying to detect. We defined the Bayesian detection threshold as the intersection of the sky (or theoretical prediction) and object pixel distributions (*i.e.* where the object pixel flux becomes dominant). To convert this empirical threshold for use with SExtractor, we scaled the χ^2 threshold (which is a flux per pixel value) into a surface brightness threshold (which is in magnitudes per square arcsecond).

The infrared images were cataloged separately due to their radically different field-of-view and pixel scale. The catalog was generated using SExtractor as before but in single image mode (*i.e.* the detection image was also the measurement image). In order to maximize the number of detections, we utilized the exposure image generated by DIMSUM during the data reduction (see §2.1.3) to provide a weight map in order to properly determine object parameters in an image with varying signal-to-noise (due to the different total integration times in different pixels).

All of our resultant analyses use the total magnitudes calculated by SExtractor. The optical magnitudes were, by design, matched apertures which reduces the scatter in any photometric redshift technique. Since the K' band images were not co-registered with the optical images, the aperture can be slightly different. However, since the total apertures were rather large in angular extent, any “aperture effects” on our resulting analysis should be small ($\lesssim 0.02^m$) compared to the more dominant effects of photometric errors.

2.3. Cross-identifications

The last step in preparing these data for analysis was to combine the optical imaging, near-infrared imaging, and the spectroscopic observations into a single dataset for each cluster field. Since the original spectroscopic targets were determined from a separate catalog, we first cross-matched the spectroscopic catalog with the optical catalog using a growing annulus technique where the angular distance ψ was determined using the formula

$$\psi = \arccos(\sin(\phi_s) \sin(\phi_p) + \cos(\phi_s) \cos(\phi_p) \cos(\theta_s - \theta_p))$$

where the angles ($\theta \equiv$ Declination, $\phi \equiv$ Right Ascension) have been properly converted into radians, and the subscript, s , refers to spectroscopic target and the subscript, p , refers to photometric object. In all cases, the match-up occurred for very small angles because spectroscopic targets were selected from the optical images.

The cross-identification between the infrared and optical catalogs, however, was slightly more complicated, although it was done in an identical manner. This was due to the different telescopes and detectors used during the observations, and the corresponding geometric distortions present between the two catalogs. Furthermore, the variation of the spectral energy distributions of the sources in our sample between the I and K' bands can be quite large, especially for galaxies at

relatively high redshift. As a result, some objects in each catalog remained unmatched below the angular limit which is approximately the confusion beam width (approximately five arcseconds).

3. Empirical Photometric Redshift

The technique that we have developed for determining cluster membership requires redshift estimates for all galaxies in the field. Although the technique is independent of the actual redshift estimation technique, we have used the empirical photometric redshift technique (Brunner *et al.* 1999) to generate redshift estimates for all galaxies in our sample. This is the result of the simplicity of the empirical technique in determining redshifts for a photometric sample of galaxies for which an adequate training set exists. Furthermore, the empirical technique, since it is based only on the data under investigation, is more robust than alternative techniques to uncertainties in the spectral energy distributions of galaxies. These alternative techniques, such as template-based methods, could also be used, as long as a realistic estimate of the error in the estimated redshift can be determined.

The empirical photometric redshift technique requires a calibration sample to determine the coefficients of the empirical relation. For this work, we have used the spectroscopic data which was acquired as part of the original observational campaign to determine the cluster velocity dispersions (Postman *et al.* 1998, 2000). The reliability (*i.e.* the inverse of the intrinsic error) of a spectroscopic redshift is generally quite high, with quoted errors often measured in the tenths of a percent (*i.e.* $\delta < 0.001$). In reality, however, a redshift is accurate only when the spectral identification is also accurate. As a result, we restricted the spectroscopic calibrators to include only objects with redshifts that are determined by at least two spectral lines, *i.e.* a quality of 2 or higher (for details, see Postman *et al.* 1998). The next step was to restrict the sample to those objects which were below the 10% photometric error limit, which did not have bad detection flags (*e.g.*, object near edge of frame, incomplete aperture data), and which were below our high redshift cut-off of $z = 1.5$. We also removed one additional galaxy which, having an $E + A$ spectrum (Dressler & Gunn 1983, 1992; Zabludoff *et al.* 1996), skewed the results of our calibration for normal galaxy spectra (which are the dominant population in our sample). The final spectroscopic calibration data consisted of 130 galaxies from five different cluster fields.

With the final calibration sample, we determined a fourth order polynomial fit to the four magnitudes B, R, I , & K' , and the spectroscopic redshift. Our sample of 130 calibrators is nearly twice the number of coefficients required (a fourth order polynomial in four variables has 70 coefficients); we are, therefore, properly constraining the degrees of freedom when determining the coefficients of our polynomial fit. From Figure 1, there are no obvious systematic variations in our calculated relationship, which has an intrinsic dispersion (the standard deviation of the residual differences for the calibrating sample) of $\sigma_z = 0.072$. In addition, the distribution of the residuals (see Figure 2) are approximately Gaussian in shape.

3.1. Estimating Photometric Redshift Errors

In order to reliably determine cluster membership, we also need to have an estimate for the error in our photometric redshift calculation. While the measurement of the intrinsic dispersion in our relationship provides one estimate (which is commonly used throughout the relevant literature, *e.g.*, Kodama *et al.* 1999), we have also developed an alternative, extrinsic estimate. Briefly, the intrinsic error is calculated directly from any available spectroscopic redshifts; that is, it is simply the dispersion in the derived relationship between spectroscopic and photometric redshifts. Extrinsic errors, on the other hand, are calculated in a Monte-Carlo fashion, accounting for all known measurement uncertainties.

Following Brunner *et al.* (1999), we derive extrinsic redshift error estimates for all galaxies in our dataset using a Monte-Carlo technique to simulate our uncertainty in both the observables (*i.e.* flux measurements), as well as our sampling of the galaxy distribution in the $B, R, I,$ & K' four-dimensional flux space. Specifically, we use a bootstrap with replacement algorithm to randomly draw a new set of calibrating galaxies from the original training set. This algorithm allows for duplicate galaxy entries and is designed to emphasize any incompleteness in the sampling of the true distribution of galaxies in the four dimensional space $B, R, I,$ & K' by the calibration redshifts. Furthermore, the magnitudes of the newly derived calibrating sample were drawn from a Gaussian probability distribution function with the mean given by the measured magnitude and sigma by the magnitude error. This accounts for any uncertainties in the flux measurements.

This technique was used to generate one hundred different realizations of the photometric redshift relationship. For each different realization (all of which form our ensemble), a photometric redshift was calculated for every galaxy in the photometric catalog. As a result, this produces one hundred different redshift estimates for each galaxy. By applying a quantile cut, we can approximate the redshift distribution for each individual galaxy by a Gaussian. Therefore, the error in the photometric redshift for each object was defined by $\sigma_z = (Q5 - Q2)/2.0$, where $Q5$ and $Q2$ refer to the fifth and second quantiles of the distribution of each galaxy's estimated redshift, respectively (see Brunner *et al.* 1999). Together, our original photometric redshifts and redshift error estimates completely define the photometric redshift distribution for each individual galaxy.

Of the two types of redshift error estimates, the intrinsic error is by far the most commonly used (*e.g.*, Kodama *et al.* 1999), as it is the easiest to calculate. The extrinsic error, however, does a better job of quantifying the actual error in the redshift estimate of an individual galaxy, which can be both smaller or considerably larger than the intrinsically estimated global error (see Figure 15 in Brunner *et al.* 1999). Fundamentally, the extrinsic method provides an error estimate separately for each individual galaxy, while the intrinsic method provides only a global estimate.

4. Cluster Membership

While the optimal technique for unambiguously determining cluster membership is to obtain spectroscopic redshifts for all sources in the field, this process can be prohibitively expensive in telescope time allocation, especially at relatively high redshifts ($z > 0.5$). As a result, many previous studies (*e.g.*, Aragón-Salamanca *et al.* 1993; Lubin 1996; Smail *et al.* 1997; Dressler *et al.* 1997; Couch *et al.* 1998; Stanford *et al.* 1998; Lubin *et al.* 1998) have utilized a background contamination estimator in order to statistically quantify both the number of galaxies which belong to a given cluster and the morphological fraction of the cluster members. In addition to possible systematic effects which are implicit in using techniques of this type, background corrections provide no information on the likelihood of an individual galaxy being a member of a cluster.

Photometric redshifts, however, provide a relatively inexpensive redshift estimate; therefore, they can be used to estimate cluster redshifts (*e.g.*, Gal *et al.* 2000) and to determine likely cluster members (Kodama *et al.* 1999; Lubin & Brunner 1999). Previous techniques to select cluster members based on photometric redshifts (*e.g.*, Kodama *et al.* 1999) are based on a simplistic technique for defining galaxy cluster members. Basically, any galaxy which lies within a redshift shell centered on the galaxy cluster’s redshift (*i.e.* $z_c \pm \delta_z$) are identified as members. Because photometric redshifts have a large uncertainty (generally a factor of ten to fifty higher than spectroscopic redshifts), a large redshift shell (*e.g.*, $\delta_z \approx 0.05$) is used to identify likely cluster members. While certainly useful, this approach does not provide a reliable means for identifying line-of-sight contaminating galaxies.

As a result, we have developed an alternative technique which relies on the probabilistic interpretation of a photometric redshift to determine cluster membership. We define the probability density function, $\Phi(z)$, for an individual galaxy’s redshift to be a Gaussian probability distribution function with mean (μ) given by the estimated photometric redshift and standard deviation (σ) defined by the estimated error in the photometric redshift.

$$\Phi(z) = \frac{1}{\sigma\sqrt{2\pi}} e^{\left(-\frac{(z-\mu)^2}{2\sigma^2}\right)}$$

Using this interpretation, we can calculate the probability that a galaxy has an actual redshift within a given redshift interval.

$$\begin{aligned} P(Cluster|z_c, \Delta z, \mu, \sigma) &= N \int_{z_c - \frac{1}{2}\Delta z}^{z_c + \frac{1}{2}\Delta z} \Phi(z) dz \\ &= N \int_{z_c - \frac{1}{2}\Delta z}^{z_c + \frac{1}{2}\Delta z} \frac{1}{\sigma\sqrt{2\pi}} e^{\left(-\frac{(z-\mu)^2}{2\sigma^2}\right)} dz \\ &= \frac{N}{2} (\gamma[\frac{1}{2}, z_H] - \gamma[\frac{1}{2}, z_L]) \end{aligned}$$

where N is a suitable normalization factor, z_c is the cluster redshift, Δz is the width in redshift

space which you are sampling, the limits of integration are

$$z_H = \frac{(z_c + \frac{1}{2}\Delta z) - \mu}{\sqrt{2} \sigma}, z_L = \frac{(z_c - \frac{1}{2}\Delta z) - \mu}{\sqrt{2} \sigma},$$

and γ is the incomplete gamma function. (Of course, $\gamma[\frac{1}{2}, z]$ is also known as the error function, $\text{erf}(z)$).

Within this formalism, the only undeclared quantity is σ or, alternatively, the uncertainty in the estimated redshift for a given galaxy. In our framework, this value can either be determined from the intrinsic error in our photometric redshift relation or in a separately calculated extrinsic error. As a result, this approach is strongly dependent on the actual technique used to estimate the photometric redshift error and corresponding redshift error. In this paper, we have applied this technique using empirically derived photometric redshifts since we have a well-defined calibration dataset of spectroscopic redshifts. Empirically defined photometric redshifts are much less sensitive to uncertainties in the shape and the evolution with redshift of the spectral energy distribution of galaxies than competing techniques such as template photometric redshifts (Brunner 1997).

On the other hand, the method we have introduced can easily be adapted to work with alternative redshift estimation procedures, including template photometric redshift algorithms, by utilizing the derived dispersion estimate. The empirical-based techniques do have shortcomings; most notably, the requirement of a high quality training set and the fundamental limitation that any resultant analysis is limited to the same region of flux space delineated by the training set of calibration redshifts. In our case, the spectroscopic survey of Oke *et al.* (1998) provides a wonderful training set, which completely samples the region in flux space which encompasses the vast majority of cluster galaxies. When this is not the case, template based photometric redshift estimation methods, which can be applied to data where there are no calibrators, are required. In this case, however, extreme care must be used to minimize any systematic effects, such as morphological variation of the redshift error estimates or template incompleteness.

By using the calibration galaxies as a training set, we can empirically determine the optimal probability value which provides the threshold for cluster membership. This can be tuned to either maximize the completeness or minimize contamination. In this paper, our sample is small enough that a simple visual threshold determination is sufficient; however, there is no reason that a more powerful maximum likelihood or regression analysis technique could not be employed, especially for larger datasets (*e.g.*, the SDSS). Furthermore, additional information (such as evolutionary color tracks) can be used to select likely cluster members which can be used to provide a bootstrap estimator for the probability threshold.

As a demonstration of this technique, we have applied this procedure to the data described earlier in this paper. We consider two clusters from our survey (see Section 2 for more information), the first is Cl 0023+0423 at a redshift of $z = 0.84$ (Postman *et al.* 1998; Lubin, Postman & Oke 1998; Lubin *et al.* 1998), and the second is Cl 1604+4321 at a redshift of $z = 0.92$ (Postman *et al.* 2000; Lubin *et al.* 2000). These two clusters provide a useful demonstration because the first

cluster is well sampled by our dataset, while the second cluster pushes the photometric limits of our data. Since the utility of this technique is so strongly dependent on the exact method used for estimating the redshift and redshift error for every galaxy in the field, we have intentionally relegated a more complete discussion of the application of this technique to our own data to a later, more targeted paper (Lubin *et al.* 2000).

In Figures 3 and 4, we display the results of applying this technique to the spectroscopic targets in the Cl 0023+0423 cluster field, as well as the full photometric sample for this field. In both cases, we used the intrinsic error of the photometric redshift relationship as our redshift error. From the first panel, we clearly do quite well (*i.e.* 100% completeness with no contamination). Of course, translating this success to the full sample is not guaranteed; however, as long as our calibration sample adequately samples the four dimensional flux space occupied by the galaxies in our full sample (*i.e.* we have a fair and unbiased training set), there is no reason to expect significant variation from these results.

In Figures 5 and 6, we show the results of applying this technique to the spectroscopic targets in the Cl 1604+4321 cluster field, as well as the entire photometric sample for this cluster. This time, however, we have used the extrinsic error which is calculated independently for each galaxy. By judiciously selecting the probability threshold, we can maximize the completeness (which is $\approx 88\%$), while minimizing the contamination (which is $\approx 21\%$). While we would clearly prefer full completeness and no contamination, this cluster demonstrates one of the strengths of our technique, namely the ability to empirically quantify both our completeness and contamination.

In fact, our technique predicts 37 cluster members within the field of view of our combined image (see Figure 6). If we use the predictions of deep number counts (*e.g.*, Driver *et al.* 1995; Smail *et al.* 1995; Abraham *et al.* 1996) to estimate the contamination due to foreground and background galaxies, we estimate there should be 33 ± 14 cluster members in the image (note the large uncertainty in this statistical calculation), which is the exact number that we find after correcting for contamination and incompleteness [*i.e.* $37 \times (1 - 21\%) / 88\% = 33$]. We have made this comparison with the statistical background correction simply in order to show that we are finding a reasonable number of cluster galaxies; however, unlike the background correction technique, we have explicitly identified the likely cluster members.

5. Discussion

In this paper, we have presented a novel technique for the probabilistic determination of cluster membership based solely on photometric redshift and redshift error estimates. Our technique can be tuned to either maximize the completeness of cluster member identification (*i.e.* identify all actual cluster members), or, alternatively, to minimize the contamination due to foreground and background galaxies in the field. Furthermore, this technique provides a robust estimation for both the completeness and contamination fractions of identified cluster members as a function of

likelihood. A comparison between our new technique with the traditional technique of statistical background correction shows remarkable agreement, with the caveat that our technique actually identifies the galaxies which are cluster members.

The results in this paper are based on an empirical photometric redshift estimation, which we have used because (a) we have a reliable training set from our extensive spectroscopic survey, and (b) these photometric redshifts are less sensitive to uncertainties in spectral evolution which can affect other redshift estimation techniques. Alternative redshift estimation techniques, however, can easily be incorporated into the algorithm, as all that is needed is a redshift estimate and a corresponding redshift error estimate. In the case of template photometric redshifts, the redshift error could be determined from either the intrinsic dispersion in the photometric redshift relation, an interpolation over the χ^2 goodness-of-fit parameter, or even more appropriately through a combination of the χ^2 parameter and a Monte-Carlo bootstrap approach to mimic photometric uncertainty and template incompleteness. In this case, however, caution must be used to minimize any possible systematic effects which might depend on various fundamental assumptions, such as the spectral type.

The only free parameter in the entire technique is the probability threshold used to determine cluster membership. Optimally, as we have done in this paper, a training set of spectroscopically confirmed cluster members can be used to empirically set the threshold value. When this is not the case, alternative techniques, such as color-selection to identify the early-type sequence at the appropriate redshift, can be used to identify likely cluster candidates. On the other hand, the expected number of cluster candidates can be calculated from the statistical background correction arguments. This expected number of cluster members can be used as an independent estimator as we can set the probability threshold value to reproduce the estimated number of cluster galaxies.

Based on our work, we believe that photometric redshifts are an ideal way to study the galaxy populations in high-redshift clusters. For a large number of the tests of common cluster properties (*e.g.*, the Morphology-Density relationship), this method eliminates the need for extensive spectroscopic surveys and the uncertainty of estimating the background contamination. As an additional example of the utility of this approach, consider the magnitude-limited, spectroscopic survey used in this analysis. We can approximate the total number of spectroscopic targets observed by multiplying the number of clusters used in this analysis (five) by the approximate number of targets per cluster field (130), implying that a total of 650 objects were observed spectroscopically. The redshift identification success rate was nearly 77%. Of these redshifts, 50%–85% belong to non-cluster galaxies. These numbers imply that the spectroscopic survey was only 12%–38% efficient in identifying cluster candidates, depending on the richness of the cluster.

In addition, our technique provides the ability to tune the cluster candidate identification to either maximize the completeness or, alternatively, to minimize the contamination. As a practical example, maximizing completeness is essential for any observational program which is interested in completely sampling the cluster (*e.g.*, spectroscopic targeting). On the other hand, minimizing contamination is important for selecting a characteristic set of cluster members for a detailed

study of cluster member properties (*e.g.*, the Morphological fraction or the Morphology-Density relationship; Lubin *et al.* 2000). Furthermore, if a training set of spectroscopically confirmed galaxies is available, we can actually characterize the percentages of both the completeness and contamination that we expect in our final cluster candidate catalog.

Like any photometric redshift based technique, our technique is limited in its efficacy by the quality of the photometric data used in the analysis. However, our technique can be applied using a variety of photometric redshift estimation methods. Therefore, we expect that, in the near future, we will be able to fully utilize the capabilities of this technique for cluster research.

We are very grateful to Bev Oke and Marc Postman for the enormous time and effort that they put into obtaining and reducing all of the data used in this paper. We also wish to thank the anonymous referee for a thorough reading of the original paper and many interesting comments. This research has made use of NASA’s Astrophysics Data System Abstract Service. LML is supported by NASA through Hubble Fellowship grant HF-01095.01-97A from the Space Telescope Science Institute, which is operated by the Association of Universities for Research in Astronomy, Inc., under NASA contract NAS 5-26555.

REFERENCES

- Abraham, R.G., van den Bergh, S., Glazebrook, K., Ellis, R.S., Santiago, B.X., Surma, P. & Griffiths, R.E. 1996, *ApJ*, 107, 1.
- Aragón-Salamanca, A., Ellis, R.E., Couch, W.J., & Carter, D. 1993, *MNRAS*, 262, 764.
- Bertin, E., & Arnout, S. 1996, *A&AS*, 117, 393.
- Brunner, R.J. 1997, PhD. Thesis, The Johns Hopkins University.
- Brunner, R.J, Connolly, A.J., Szalay, A.S., & Bershad, M.A. 1997, *ApJ*, 482, L21.
- Brunner, R.J, Connolly, A.J., & Szalay, A.S. 1999, *ApJ*, 516, 563.
- Brunner, R.J, Connolly, A.J., & Szalay, A.S. 2000, *ApJ*, in press.
- Connolly, A.J., Szalay, A.S., & Brunner, R.J. 1998, *ApJ*, 499, L125.
- Couch, W.J., Barger, A.J, Smail, I., Ellis, R.E., & Sharples, R.M. 1998, *ApJ*, 497, 188.
- Dressler, A. & Gunn, J.E. 1983, *ApJ*, 270, 7.
- Dressler, A. & Gunn, J.E. 1992, *ApJS*, 78, 1.
- Dressler, A., Oemler, A., Couch, W.J., Smail, I., Ellis, R.E., Barger, A., Butcher, H., Poggianti, B.M., & Sharples, R.M. 1997, *ApJ*, 490, 577.

- Driver, S.P., Windhorst, R.A., Ostrander, E.J., Keel, W.C., Griffiths, R.E. & Ratnatunga, K.U. 1995, ApJ, 449, L23.
- Gal, R.R., de Carvalho, R.R., Brunner, R., Odewahn, S.C., and Djorgovski, S.G. 2000, AJ, accepted.
- Kodama, T., Bell, E.F., and Bower, R.G. 1999, MNRAS, 302, 152.
- Landolt, A.U. 1992, AJ, 104, 340.
- Lubin, L.M. 1996, AJ, 112, 23.
- Lubin, L.M., Postman, M., Oke, J.B., Ratnatunga, K.U., Gunn, J.E., Hoessel, J.G. & Schneider, D.P. 1998a, AJ, 116, 584.
- Lubin, L.M., Postman, M., & Oke, J.B. 1998b, AJ, 116, 643.
- Lubin, L.M., & Brunner, R.J. 1999, In R. Weymann, L. Storrie-Lombardi, M. Sawicki, & R. Brunner, editors, *Photometric Redshifts and High-Redshift Galaxies*, number 191 in ASP Conference Series.
- Lubin, L.M., Postman, M., Oke, J.B., Brunner, R.J., Gunn, J.E., Hoessel, J.G. & Schneider, D.P. 2000, AJ, in preparation.
- Oke, J.B., *et al.* 1995, PASP, 107, 375.
- Oke, J.B., Postman, M., & Lubin, L.M. 1998, AJ, 116, 584.
- Persson, S.E., Murphy, D.C., Krzeminiski, W., Roth, M., & Rieke, M.J. 1997, AJ, 116, 2475.
- Postman, M., Lubin, L.M., & Oke, J.B. 1998, AJ, 116, 560.
- Postman, M., Lubin, L.M., & Oke, J.B. 2000, in preparation.
- Smail, I., Hogg, D.W., Yan, L., & Cohen, J.C. 1995, ApJ, 449, 105.
- Smail, I., Dressler, A., Couch, W.J., Ellis, R.E., Oemler, A., Butcher, H., & Sharples, R.M. 1997, ApJS, 110, 213.
- Stanford, S.A., Eisenhardt, P.R., & Dickinson, M. 1998, ApJ, 492, 461.
- Szalay, A.S., Connolly, A.J., & Szokoly, G.P. 1998, AJ, 117, 68.
- Williams, R.E., Blacker, B., Dickinson, M.E., Dixon, W., Ferguson, H.C., Fruchter, A.S., Giavalisco, M., Gilliland, R.L., Heyer, I., Katsanis, R., Levay, Z., Lucas, R.A., McElroy, D.B., Petro, L., Postman, M., Adorf, H., & Hook, R. 1996 AJ, 112, 1335.
- Weymann, R., Storrie-Lombardi, L., Sawicki, M., & Brunner, R. 1999, editors, *Photometric Redshifts and High-Redshift Galaxies*, number 191 in ASP Conference Series.

Zabludoff, A.I., Zaritsky, D., Lin, H., Tucker, D., Hashimoto, Y., Sheckman, S.A., Oemler, A., & Kirshner, R.P. 1996, ApJ, 466, 104.

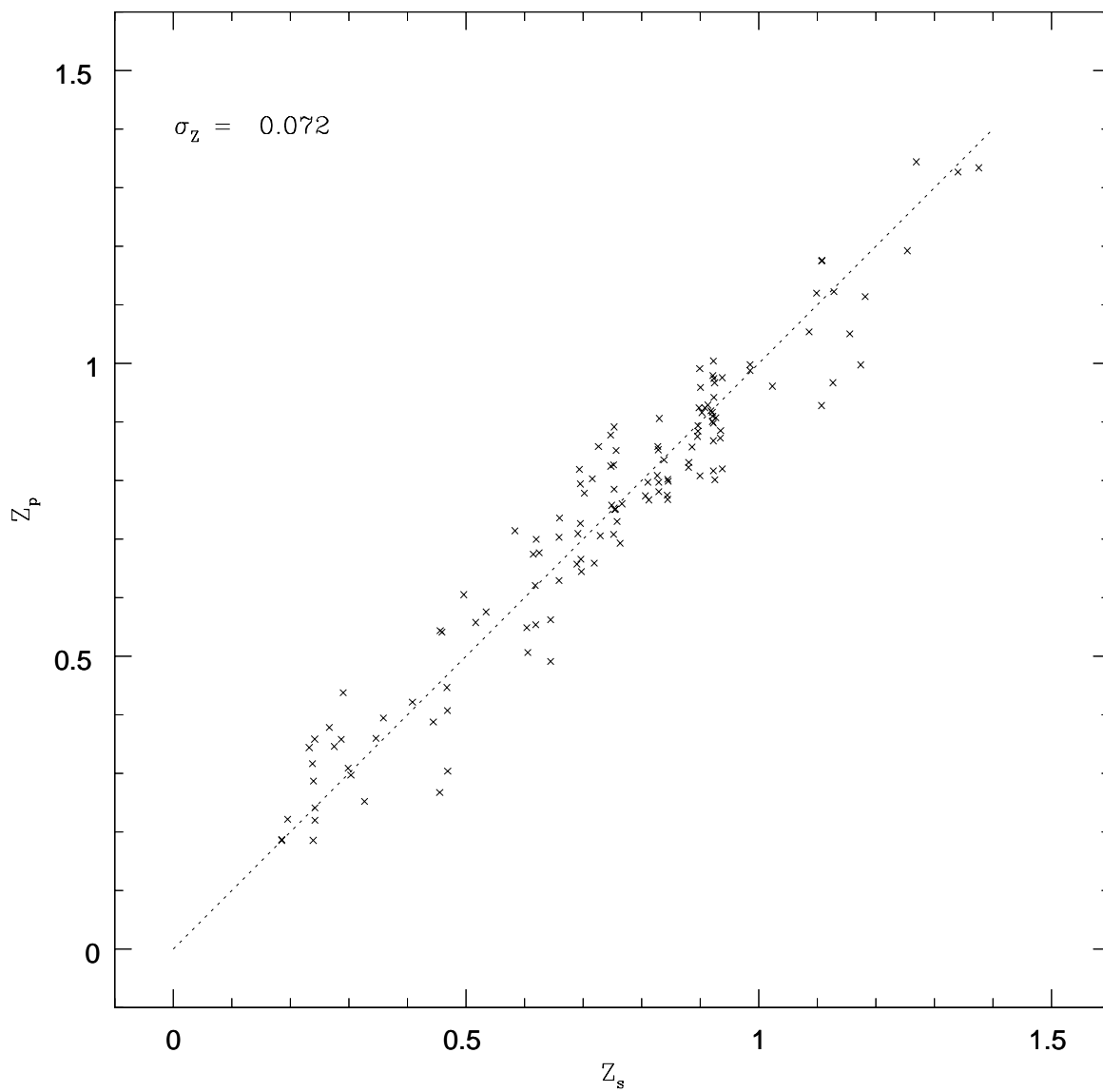


Fig. 1.— The correlation between the photometric and spectroscopic redshifts for the entire calibration sample. The straight line is of unit slope and is not a fit to the actual data.

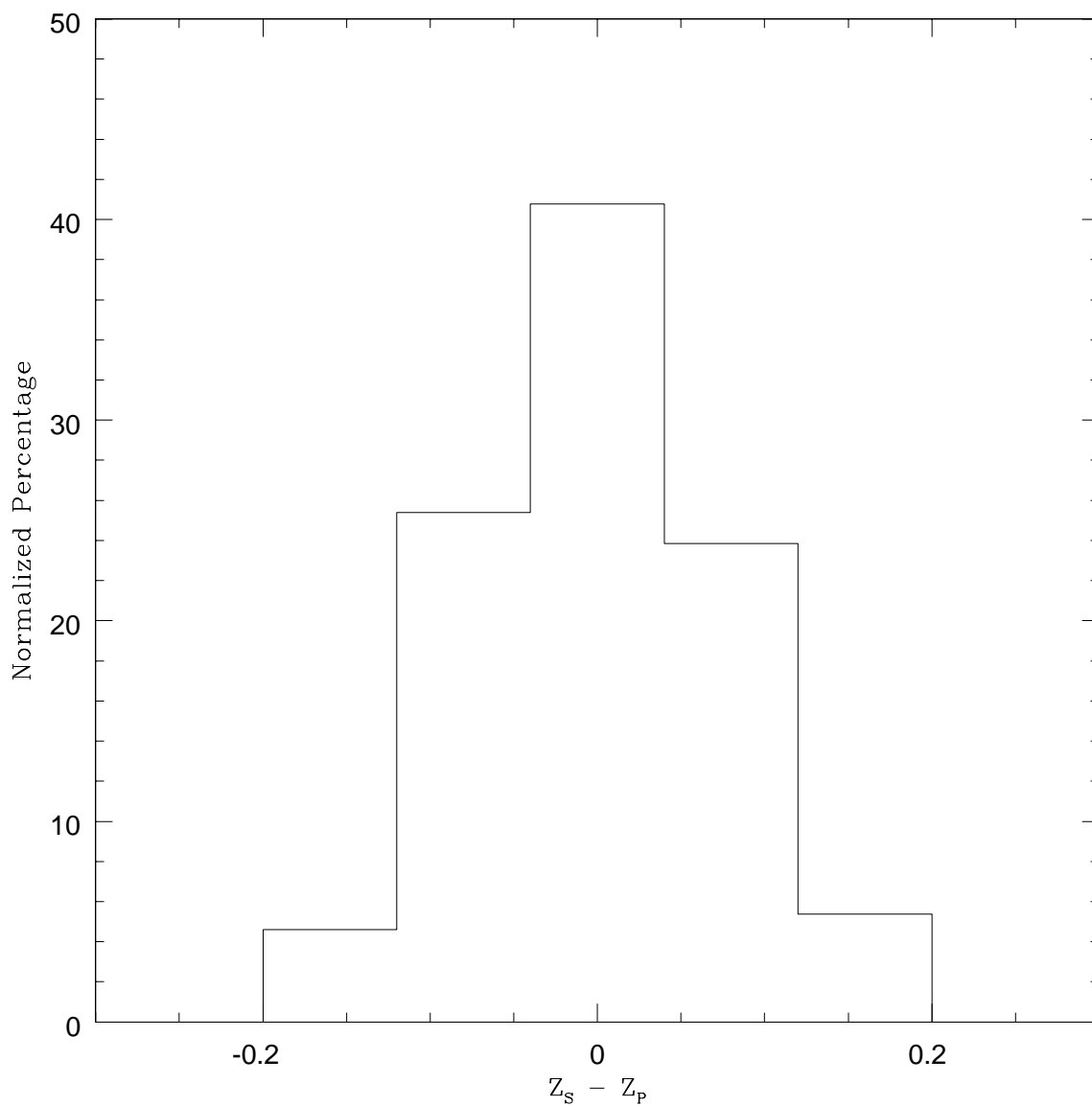


Fig. 2.— A histogram of the residual differences between photometric and spectroscopic redshifts for the entire calibration sample, which is approximately Gaussian in shape. The bin width was chosen to approximate the measured intrinsic dispersion in our relationship.

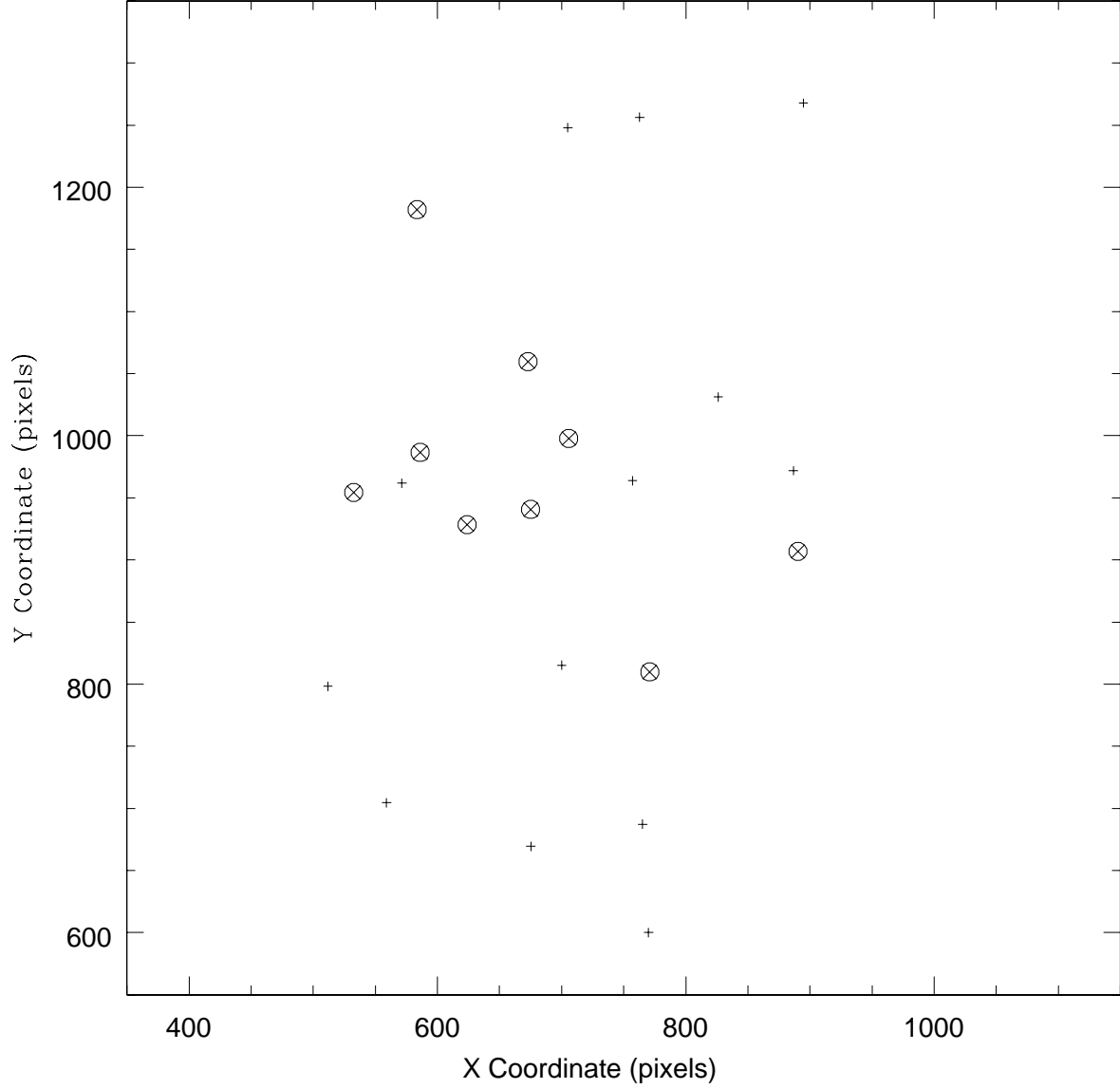


Fig. 3.— Results for the field of Cl 0023+0423. A plot displaying the locations of calibrating galaxies in the image (the pixel scale is 0.215 arcsec/pixel). The spectroscopically confirmed cluster members are indicated by \circ , photometrically classified cluster members are indicated by \times , and $+$ indicates field galaxies which are additional calibrators for the photometric redshift relation. With the probability cut selected for this figure, we have 100% completeness and 0% contamination.

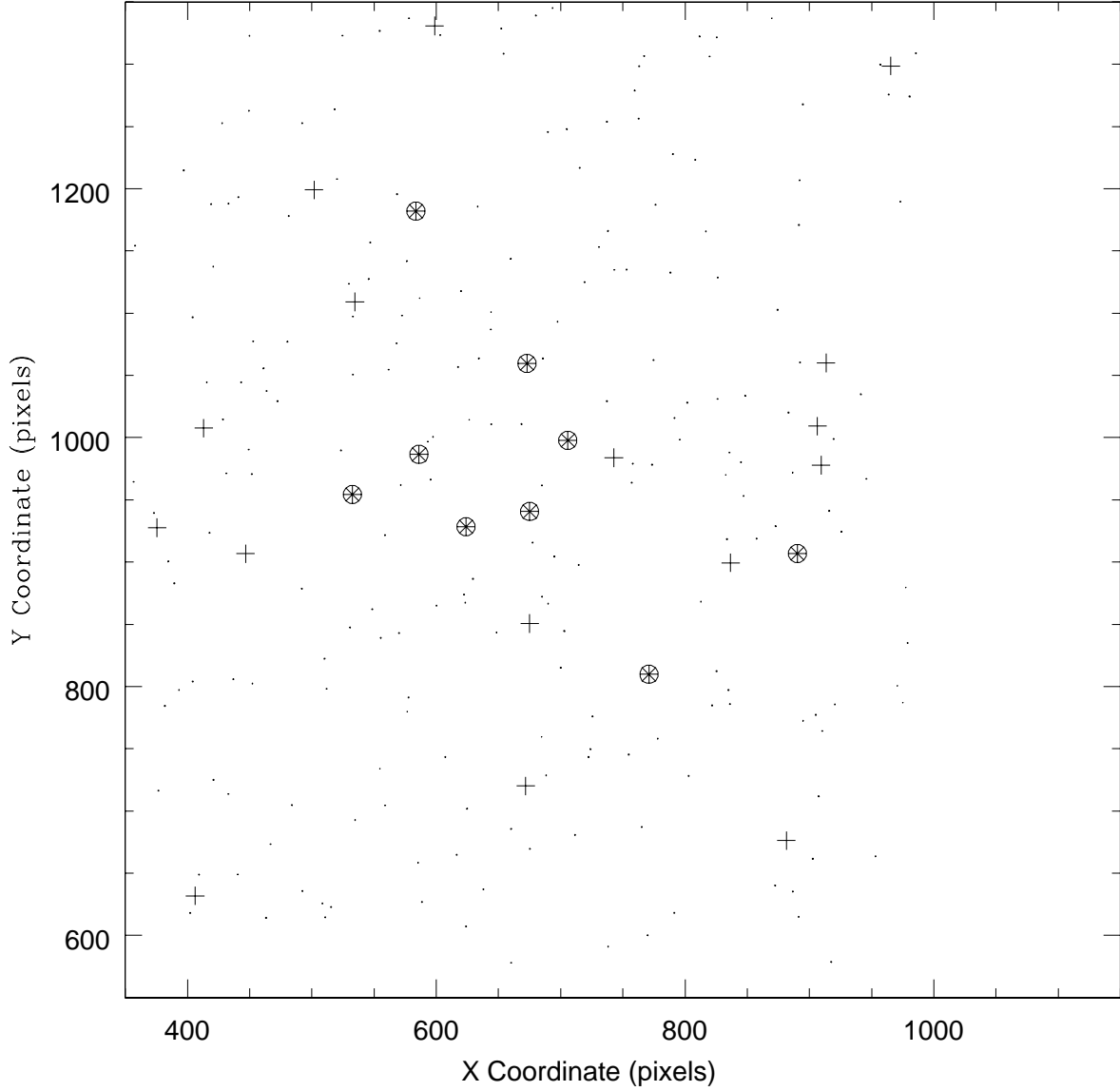


Fig. 4.— Results for the field of Cl 0023+0423. A demonstration of the application of this technique to the full photometric catalog. Cluster candidates are indicated as before (both spectroscopic and photometric), while new cluster candidates are indicated by + and general field galaxies are indicated by the dots. After correcting for contamination and incompleteness, the number of cluster members determined through our photometric redshift technique agrees with the number predicted by statistically correcting for background counts.

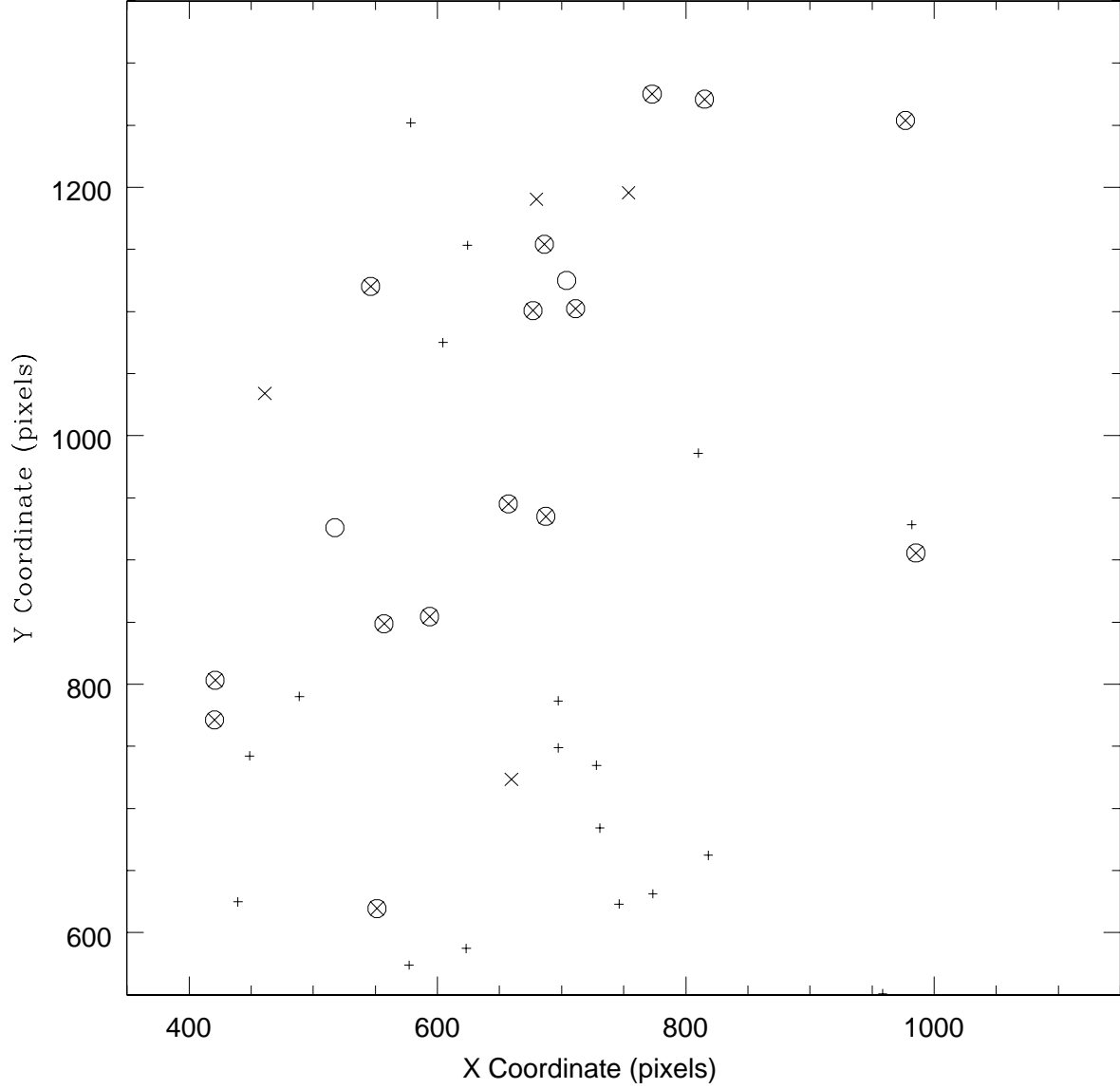


Fig. 5.— Results for the field of Cl 1604+4321. A plot displaying the locations of calibrating galaxies in the image (the pixel scale is 0.215 arcsec/pixel). The spectroscopically confirmed cluster members are indicated by \circ , photometrically classified cluster members are indicated by \times , and $+$ indicates field galaxies which are additional calibrators for the photometric redshift relation. With the probability cut selected for this figure, we have $\approx 88\%$ completeness and $\approx 21\%$ contamination.

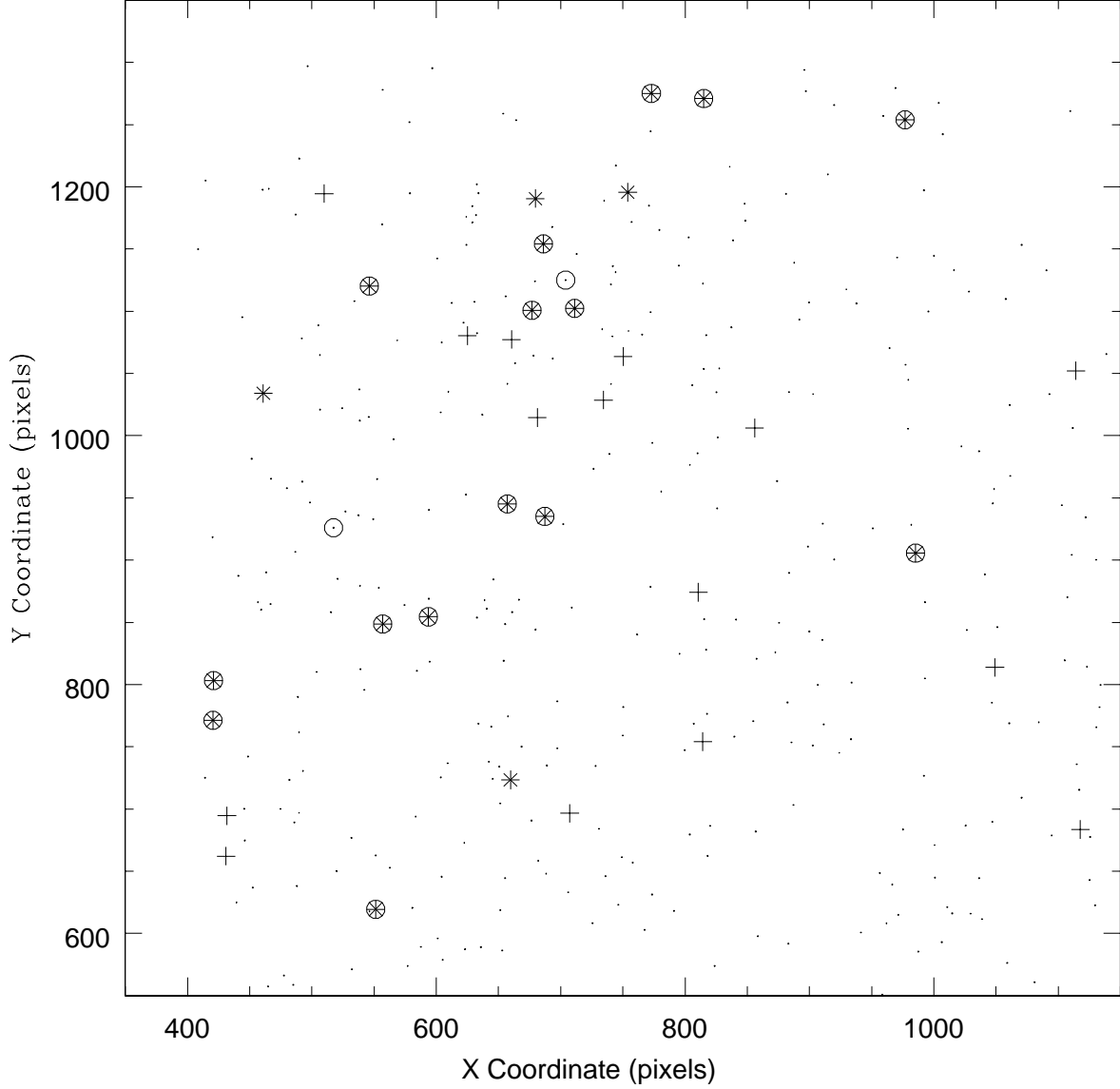


Fig. 6.— Results for the field of Cl 1604+4321. A demonstration of the application of this technique to the full photometric catalog. Cluster candidates are indicated as before (both spectroscopic and photometric), while new cluster candidates are indicated by + and general field galaxies are indicated by the dots. After correcting for contamination and incompleteness, the number of cluster members determined through our photometric redshift technique agrees with the number predicted by statistically correcting for background counts.